World Scientific
www.worldscientific.com

A Method for Determining the Fundamental Site Period and the Average Shear Wave Velocity

Kanat Burak Bozdogan [ID]*

Department of Civil Engineering Canakkale Onsekiz Mart University
Terzioglu Kampusu, Canakkale 17100, Turkey
kbbozdogan@comu.edu.tr

Erdinc Keskin [ID]

Department of Civil Engineering
Kırklareli University, Kayali Kampusu
Kırklareli 39100, Turkey
erdinckesin@klu.edu.tr

The soil–structure interaction plays a crucial role in determining the displacement and internal forces of multi-story buildings subjected to strong ground motion. One of the critical dynamic characteristics influencing soil–structure interaction is the fundamental site period and the average shear wave velocity associated with it. This study introduces an original equation to determine these parameters. In addition, for the first time in the literature, the version of the Rayleigh method used for finding the fundamental periods of buildings is used to find the fundamental site period. The soil is modeled as an equivalent shear beam to obtain the proposed equation. The peak displacement is obtained by acting the soil mass as an external load on the equivalent shear beam. For single-layer soil, the fundamental site period is proportional to the square root of the peak displacement of the equivalent shear beam. The least squares method generalizes the proposed relation for single-layer soils to multi-layer soil profiles. Modified Finite element Transfer matrix method is used for calibration in the least squares method. The equations used in the literature and earthquake codes for determining the fundamental site period and average shear velocity are tested on various examples, and it is shown that the method proposed in this study, along with the Rayleigh method, gives better results than these equations. The performances of these two methods and the five commonly used equations are tested and compared on different soil profiles. Transfer functions, Finite Element Method (SAP200) and Modified Finite Element Transfer Matrix Method are used for verification. For all soil profiles, the results obtained from the transfer function, Finite Element Method (SAP200) and Modified Finite Element Transfer Matrix Method are found to be in agreement. The true percent relative error found in the results obtained with the proposed method is 4.47%.

Keywords: Average shear wave velocity; one-dimensional analysis; fundamental site period; soil-structure interaction; site effects.

*Corresponding author.

1. Introduction

The soil characteristics upon which buildings are constructed play a significant role in causing earthquake damage. Soils transfer the effects of ground motion to the surface by increasing or decreasing it, a phenomenon commonly referred to as the site effect. Numerous studies have examined the site effect; some of these findings are summarized below.

Many studies have examined the selection of earthquake records entered as input in seismic site response analysis [Genovese *et al.*, 2019a,b, 2020, 2023a,b]. Zhang and Zhao [2021] analyzed seismic ground motions recorded in nearby soil and rock sites, statistically comparing the Fourier spectral ratio (FSR) and the response spectral ratio (RSR). The study revealed that while the average RSR and FSR are generally similar and peaked at the same period, significant differences are observed around the peak values. Specifically, the FSRs are consistently higher than the RSRs. Parla and Somala [2022] investigated the effect of source mechanism parameters, such as fault strike, slope, slope angle, and moment magnitude (Mw), on ground amplification in basins, a departure from previous studies. The study emphasizes the importance of considering detailed focal parameters when examining basin amplification. Yu *et al.* [2023], using the three-dimensional Sichuan basin model they created, examined the factors affecting basin amplification using the spectral analysis method. The study also examined the effect of the site soil. Yuebing *et al.* [2024] compared the seismic performance of a transformer without insulation and a transformer with arranged isolation bearings. At the end of the study, it was found that the dynamic properties of the site soil significantly affected the insulation performance and the expected insulation effect in soft soils was achieved.

Another critical factor affecting the vulnerability of buildings is soil–structure interaction. Numerous studies have investigated soil–structure interaction under seismic loads, including one-dimensional site response analyses pile foundations, flexible and rigid foundations, cantilever walls, sheet piles, reinforced concrete frames, bridges, and adjacent buildings [Jiang *et al.*, 2018; Van Cao, 2018; Ngo *et al.*, 2019; Hoseini *et al.*, 2019; Sbartai, 2020; Huynh *et al.*, 2021; Raheem *et al.*, 2021; Jin *et al.*, 2021; Zhao *et al.*, 2022; Ozturk *et al.*, 2023; Haque and Ahmed Ansary, 2023; Fadayi Asiabsary *et al.*, 2023].

Important parameters that directly affect both site analyses and soil–structure interaction analyses are the fundamental site period (FSP), fundamental modal shape and the average shear wave velocity (ASWV). ASWV holds notable importance in various earthquake codes such as the National Earthquake Hazard Reduction Program (NEHRP), the Building Seismic Safety Council (BSSC), Eurocode 8: Design of Structures for Earthquake Resistance (EC8), Turkish Seismic Code (TSC), and others. It plays a crucial role in soil classification and the determination of the FSP [BSSC, 2003; Eurocode, 2004; TSC, 2018].

Numerous studies have been conducted in the literature to determine ASWV and the FSP, summarized below. Sawada [2004] highlighted the significance of

estimating the natural period of local soil deposits for seismic design purposes in buildings and infrastructure. While various simplified equations have been employed to approximate the natural period of layered ground, these equations can yield inadequate values as they typically assume a rigid bedrock. To address these limitations, the author proposed a new simplified equation based on the Reflection/ Transmission Coefficient method to more accurately approximate the natural period of layered ground on an elastic bedrock. Lee and Trifunac [2010] addressed using the ASWV in the top 30 m of soil as a parameter in seismic codes and empirical scaling equations for estimating strong ground motion amplitudes. Despite its widespread use, the authors argued that the ASWV in the top 30 m of soil may not be a meaningful or reliable parameter. Luzi *et al.* [2011] noted that soil classification for site-specific considerations in seismic engineering is commonly done using elastic response spectra. While international seismic codes often rely on the ASWV of the upper 30 m ($V_{s,30}$) for this purpose, doubts have emerged about its accuracy in predicting soil amplification. Luzi *et al.* proposed two soil classifications, introducing the soil fundamental frequency (f_0) as an alternative or complementary parameter to $V_{s,30}$. The performance of these classifications was evaluated by estimating standard deviation in ground motion prediction equations. Results show that combining $V_{s,30}$, and f_0 reduces standard deviation, and using f_0 alone also yields satisfactory results comparable to the $V_{s,30}$ based classification. Pitilakis *et al.* [2013] conducted a study presenting a global dataset comprising over 3,000 ground motion records from 536 sites across Greece, Italy, Turkey, the USA, and Japan. This dataset introduced a novel site classification system, proposing code-oriented elastic acceleration response spectra and soil amplification factors. Unlike traditional geotechnical parameters, this system incorporated the fundamental period of the site, soil deposit thickness, and ASWV into the seismic bedrock. The proposed classification system, including associated amplification factors and normalized response spectra for two seismicity levels, aimed to enhance the current EC8 soil classification. Comparative analysis with the EC8 classification system indicated that the error terms for the new classification system were consistently lower across all periods, emphasizing its improved effectiveness. Wang *et al.* [2018] proposed the FSP as an alternative to the time ASWV to 30 m (V_{s30}) for estimating site amplification in ground motion prediction equations. They introduced a simple approach for constructing continuous variation velocity models and provided analytical, numerical solutions for three cases: linear increase or decrease of SWV with depth, SWV increasing as a power of depth, and linear increase or decrease of shear modulus with depth. The study also presented seven practical methods for estimating the FSP from SWV profiles, evaluating their accuracy by comparing them with analytical solutions and empirical results. Vijayendra *et al.* [2010] aimed to assess the efficiency of different procedures for comparatively calculating the fundamental natural period of layered soil deposits. The study compared the ASWV method and Madera's procedure with the fundamental period computed from observed earthquake data for a specific soil deposit associated with an established downhole array. The fundamental period of the same

soil deposit was also estimated using free vibration analysis of a discrete multi-degree of freedom model with lumped parameters. Remarkably, the simplified procedures yield fundamental period values for the soil deposit that closely align with the observations from the recorded earthquake data. Miao and Wang [2018] investigated soil site amplification using ground motion data from KiK-net in Japan spanning January 2009 to June 2014. A moderate correlation between the FSP and surficial stiffness indicated limitations of the commonly used time-averaged velocity to 30 m (V_{s30}). The researchers established empirical relationships between high-order natural frequencies and the fundamental frequency based on 32 KiK-net stations, showing a good fit with previous theoretical frameworks. These relationships enabled the estimation of natural frequencies of the first eighth or even higher orders from the fundamental frequency. Dong-Kwan's study [2019] emphasized the importance of accurate site class determination for seismic design load and category calculation. The ASWV for multi-layer soil deposits was calculated by summing individual shear wave velocities without considering the vertical relationship of the strata. The study reviewed the transfer function for multi-layered soil deposits based on wave propagation theory, validating it through finite element models and eigenvalue analysis. Three site period estimation methods were assessed. The sum of shear wave velocities underestimated average shear wave velocities for 526 strata, showing significant deviations. The Mexican code equation overestimated ASWV, while the Japanese code equation accurately estimates them with minimal deviation. Zhang and Zhao [2019] proposed a straightforward approach to estimate the fundamental mode shape of layered soil profiles, which was a pivotal parameter in site response analysis. This approach, incorporated into the Japanese seismic code, offers engineers a convenient method to model the fundamental mode shape using basic arithmetic operations directly. Their study demonstrated that the proposed approach produces results closely aligned with actual outcomes when applied to a range of layered soil profiles. Aleshin [2021] discussed seismic microzonation, a field within engineering seismology that explored the relationship between local ground conditions and seismic vibration parameters. Within the scope of the study, the development of various earthquake codes, including NEHRP and Eurocode 8, was also highlighted. Shi *et al.* [2022] emphasized the importance of vertical ground motion in analyzing soil behavior for earthquake engineering. Due to the inadequacy of linear site response analysis concerning vertical ground motion, a comprehensive linear site response analysis was conducted using the surface-to-borehole spectral ratio technique applied to Kik-net seismic data. The study showed that the model obtained could be a reference for a multidirectional linear site response analysis. Zhang and Zhao [2022] discussed the crucial role of the FSP in constructing design spectrum models for characterizing site conditions. Contrary to the common belief that radiation damping caused by energy leaking into the bedrock does not alter the FSP for layered soil profiles on bedrock, this study revealed that radiation damping can significantly impact the FSP. The research systematically explored the effect of radiation damping on the FSP. It introduced a simple method to account for it in calculating the FSP for linear soil

profiles. The validity of the proposed method was demonstrated using numerous actual soil profiles.

While much of the existing literature focuses on estimating the fundamental site period and its corresponding mode shape, this study takes a different approach. Unlike previous studies, our research proposes a practical methodology that yields results closer to the exact solution. This study also contributes to the literature by developing a novel relationship for determining the FSP and fundamental mode shape.

This study presents an original equation to determine the fundamental site period and the average shear wave velocity, offering a significant contribution to the literature. This equation enables a fast and accurate determination of the fundamental site period compared to existing methods summarized in Table 1. In addition, in this study, for the first time in the literature, the version of the Rayleigh method traditionally used to determine the fundamental period of buildings is applied to calculate the fundamental site period, demonstrating highly accurate results closely resembling the exact solution. The method proposed in this study, along with the five equations commonly used in the literature and the Rayleigh method, are approximate methods, and three methods are employed to verify their accuracy. The starting point of all three methods is the one-dimensional wave propagation equation, which is widely accepted in the modeling of soils. By solving the wave propagation represented by a different differential equation in each layer with the help of continuity and boundary conditions, it is possible to obtain the fundamental site period value that can be named exact method. The first method employed for verification is the Modified Finite Element Transfer Matrix Method, one of the methods used to solve these differential equations, which is directly derived from the equation's solution and can be considered an exact solution. Additionally, to validate the proposed method, the Finite Element Method (FEM) is utilized. SAP2000 software, employing FEM, is employed for the analysis. Each soil layer is subdivided into four parts for modeling and analysis within SAP2000. Generally, the results obtained from SAP2000 are consistent with those from the Modified Finite Element Transfer Matrix Method. Furthermore, a third verification is conducted using transfer functions commonly employed in soil amplification analysis. Transfer Function Tool (TFT) program is used for this purpose. Results obtained from TFT align with those from the Modified Finite Element Transfer Matrix Method. This study assumes that the wave propagation in the soil is one-dimensional and the material behavior is elastic.

2. Proposed Equation for Average Shear Wave Velocity and Fundamental Site Period

This study proposes an equation for determining the FSP and the ASWV, presenting an original approach with low error rates compared to existing methods, thus enhancing the accuracy of both FSP and ASWV estimations. For this purpose,

initially, a single-layer soil and equivalent shear beam model are considered, as illustrated in Fig. 1.

Here, GA is equivalent to shear rigidity, H is the total soil thickness, V_s is shear wave velocity and ρ is soil density. The soil mass ρA is applied to the equivalent shear beam as a uniformly distributed load, single-point load and two-point load, as shown in Fig. 2.

The differential equation of the shear beam under uniformly distributed load shown in Fig. 2(a) can be expressed as

$$GA\frac{d^2y}{dz^2} = -q(z). \tag{1}$$

Equation (2) is obtained by substituting the soil mass ρA for the distributed load $q(z)$.

$$GA\frac{d^2y}{dz^2} = -\rho A. \tag{2}$$

Taking the integral of Eq. (2) yields the shear force function as follows:

$$GA\frac{dy}{dz} = -\rho Az + c_1. \tag{3}$$

Here, c_1 is the integral constant. Upon performing a second integration of Eq. (3), Eq. (4) is derived. Here, c_2 is the integral constant.
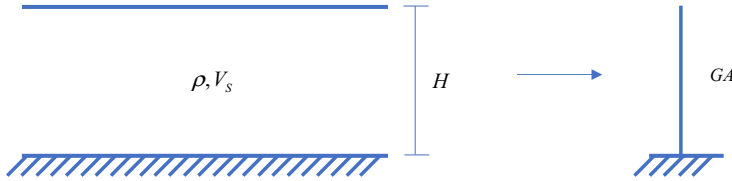

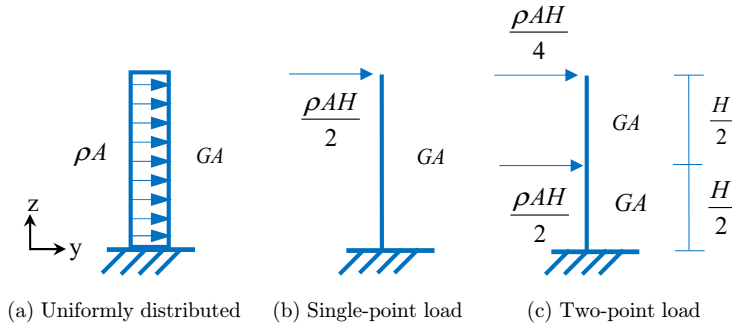Fig. 1. Single layer soil and equivalent shear beam model.

(a) Uniformly distributed   (b) Single-point load   (c) Two-point load

Fig. 2. Representation of soil mass acting as a load on the equivalent shear beam.

$$GAy(z) = -\frac{\rho A z^2}{2} + c_1 z + c_2. \tag{4}$$

The boundary conditions for Eq. (2) is given as follows:

(1) Displacement at the base equals zero:

$$y = 0 \quad \text{at } z = 0. \tag{5}$$

(2) Shear force at the top zero:

$$GA\frac{dy}{dz} = 0 \quad \text{at } z = H. \tag{6}$$

The first boundary condition yields the equation $c_2 = 0$. The second boundary condition yields the equation $c_1 = \rho AH$. Upon finding c_1 and c_2, the displacement is determined as follows:

$$y(z) = \frac{-\rho A z^2}{2GA} + \frac{\rho A H z}{GA}. \tag{7}$$

Substituting H for z in Eq. (7) yields the peak displacement as provided by

$$y(H) = \frac{\rho A H^2}{2GA}. \tag{8}$$

Equation (9) can be written for the case of a singular load applied to the top point as depicted in Fig. 2(b)

$$GA\frac{d^2 y}{dz^2} = 0. \tag{9}$$

Equation (10) is obtained by integrating Eq. (9)

$$GA\frac{dy}{dz} = c_1. \tag{10}$$

By integrating Eq. (10) once more, Eq. (11) is obtained as

$$GAy = c_1 z + c_2. \tag{11}$$

The boundary conditions for Eq. (9) are given as follows:

(1) Displacement at the base equals zero:

$$y = 0 \quad \text{at } z = 0. \tag{12}$$

(2) Shear force at the top equals singular load:

$$GA\frac{dy}{dz} = \frac{\rho A H}{2} \quad \text{at } z = H. \tag{13}$$

The first boundary condition yields the equation $c_2 = 0$. The second boundary condition yields the equation $c_1 = \frac{\rho A H}{2}$. Upon finding c_1 and c_2, the peak displacement is determined as given by Eq. (8).

For the case "c" illustrated in Fig. 2, there are two regions as follows:

(1) Within the first region:

$$0 \leq z \leq \frac{H}{2}. \tag{14}$$

For this region, the differential equation related to the function y_1 can be written as follows:

$$GA\frac{d^2y_1}{dz^2} = 0. \tag{15}$$

Equations (16) and (17) are derived through the first and second integrations, respectively.

$$GA\frac{dy_1}{dz} = c_1, \tag{16}$$

$$GAy = c_1z + c_2. \tag{17}$$

(2) Within the second region:

$$\frac{H}{2} \leq z \leq H. \tag{18}$$

The differential equation related to the function y_2 can be written as follows:

$$GA\frac{d^2y_2}{dz^2} = 0. \tag{19}$$

The first and second integrations of the differential equation given in Eq. (19) are represented with the following equations:

$$GA\frac{dy_2}{dz} = c_3, \tag{20}$$

$$GAy_2 = c_3z + c_4. \tag{21}$$

The boundary and continuity conditions for both regions can be written as follows:

(1) Displacement at the base equals zero:

$$y = 0 \quad \text{at } z = 0. \tag{22}$$

(2) Shear force at the top equals singular load at the top:

$$GA\frac{dy_2}{dz} = \frac{\rho AH}{4} \quad \text{at } z = H. \tag{23}$$

(3) Displacements are equal at the point where the two regions intersect:

$$y_1\left(\frac{H}{2}\right) = y_2\left(\frac{H}{2}\right). \tag{24}$$

(4) The sum of the shear forces at the intersection of the two regions is zero:

$$GA\frac{dy_1}{dz}\bigg|_{\frac{H}{2}} - \frac{\rho AH}{2} = GA\frac{dy_2}{dz}\bigg|_{\frac{H}{2}}. \tag{25}$$

The integral constants c_1, c_2, c_3 and c_4 are determined as follows:

$$c_1 = \frac{3\rho AH}{4}, \quad c_2 = 0, \quad c_3 = \frac{\rho AH}{4} \quad \text{and} \quad c_4 = \frac{\rho AH^2}{4}.$$

The displacement at the top is found by the following relation:

$$GAy_2(H) = c_3H + c_4. \tag{26}$$

Utilizing c_3 and c_4 in the equation reproduces Eq. (8), again. In summary, it is notable that all three load cases result in the same peak displacement, which can be calculated using Eq. (8).

SWV is defined by Eq. (27), which is well-known in soil dynamics

$$V_S = \sqrt{\frac{G}{\rho}}. \tag{27}$$

The rearrangement of Eq. (8) using Eq. (27) yields Eq. (28):

$$y_{\text{top}} = \frac{H^2}{2V_S^2}. \tag{28}$$

The period of a single layer of soil can be written as in Eq. (29):

$$T = \frac{4H}{V_S}. \tag{29}$$

The combination of Eqs. (28) and (29) will allow the expression of the FSP as depicted in Eq. (5).

$$T = 4\sqrt{2y_{\text{top}}} \cong 5.66\sqrt{y_{\text{top}}}. \tag{30}$$

In a multi-layered soil profile, the coefficient 5.66 undergoes variation. The determination of this coefficient in multi-layered soils relies on the assumption provided by

$$T = a\sqrt{y_{\text{top}}}. \tag{31}$$

Here, a represents a constant coefficient. The equivalent static loads acting on the multi-layer soil profile are illustrated in Fig. 3.

Subsequently, analyses are conducted on various soil profiles, deriving the value provided in Eq. (31) through the least squares method. In Eq. (32), the coefficient a is determined using the least squares method.
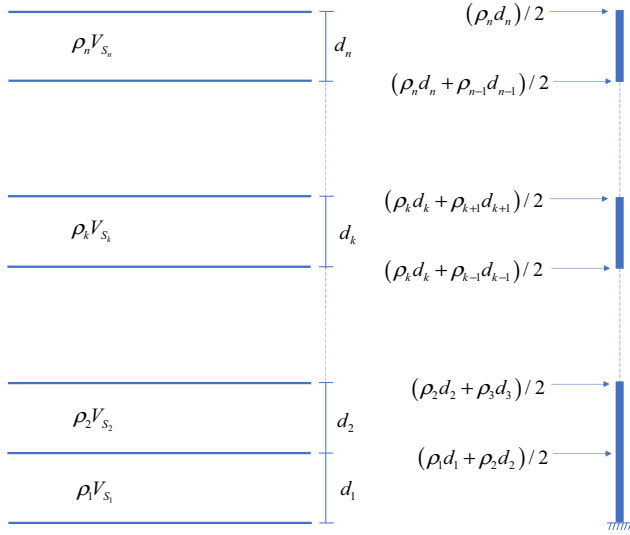
Fig. 3. Suggested method modeling and equivalent static loadings.

$$a = \frac{\sum_i^n \sqrt{y_{\text{top}_i}} T_{\text{exact}_i}}{\sum_{i=1}^n y_{\text{top}_i}}. \tag{32}$$

T_{exact_i}, represents the soil fundamental period calculated by the transfer function and the Modified Finite Element Transfer Matrix Method [Ozturk and Bozdogan, 2017] for the ith profile. i is the profile number considered, and $y_{\text{top},i}$ is the displacement at the soil surface resulting from static loading on the ith profile. The calculations yielded a value of 5.515.

Accordingly, the proposed equation is expressed by Eq. (33)

$$T = 5.515 \left[\sum_{i=1}^n \sqrt{\frac{S_i}{\rho_i V_{si}^2}} d_i \right], \tag{33}$$

S_i values provided in Eq. (33) are calculated according to Eq. (34). After calculating the FSP, the ASWV can be determined using Eq. (8).

$$S_i = \sum_{i=k+1}^n \rho_i d_i + \frac{d_k \rho_k}{2} \quad k = 1, 2, \ldots, n. \tag{34}$$

The fundamental mode shape is calculated by

$$\phi_{k_1} = \frac{\sum_{i=n-k+1}^n \frac{S_i d_i}{\rho_i V_{S_i}^2}}{\sum_{i=1}^n \frac{S_i d_i}{\rho_i V_{S_i}^2}}. \tag{35}$$
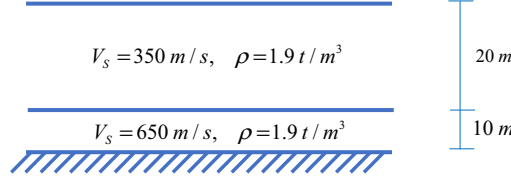
Fig. 4.   Two-layer soil profile.

An application of the proposed method is demonstrated on the two-layer soil profile depicted in Fig. 4.

S_1 and S_2 values are calculated for the two-layer soil profile using Eq. (34) as follows:

$$S_1 = \sum_{i=2}^{2} \rho_i d_i + \frac{d_1 \rho_1}{2} = 1.9 \times 20 + \frac{10 \times 1.9}{2} = 47.5,$$

$$S_2 = \frac{d_2 \rho_2}{2} = \frac{20 \times 1.9}{2} = 19.$$

Following the calculation of S_1 and S_2 values, Eq. (33) can be utilized to determine the FSP as follows:

$$T = 5.515 \sqrt{\sum_{i=1}^{2} \frac{S_i d_i}{\rho_i V_{S_i}^2}} = 5.515 \sqrt{\frac{47.5 \times 10}{1.9 \times 650^2} + \frac{19 \times 20}{1.9 \times 350^2}},$$
$$T \cong 0.26\, s.$$

The fundamental mode shape is calculated using Eq. (35):

$$\phi_{11} = \frac{\frac{19 \times 20}{1.9 \times 350^2}}{\frac{47.5 \times 10}{1.9 \times 650^2} + \frac{19 \times 20}{1.9 \times 350^2}} = \frac{1.633 \times 10^{-3}}{2.224 \times 10^{-3}} = 0.734,$$

$$\phi_{21} = \frac{\frac{47.5 \times 10}{1.9 \times 650^2} + \frac{19 \times 20}{1.9 \times 350^2}}{\frac{47.5 \times 10}{1.9 \times 650^2} + \frac{19 \times 20}{1.9 \times 350^2}} = 1,$$

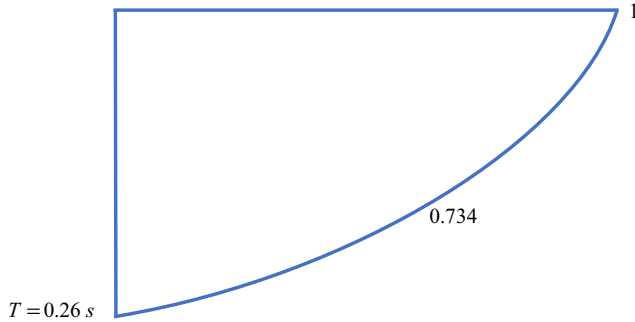$$\{\phi\}^1 = \begin{bmatrix} 0.734 \\ 1 \end{bmatrix}.$$

Fig. 5.   Fundamental mode shape for two-layer soil profile example.

The obtained fundamental mode shape for the two-layer soil profile example is represented graphically in Fig. 5.

3. Assessment of Equation Performances in Different Soil Profiles

Numerous equations in seismic earthquake codes and literature determine the FSP and ASWV, which are crucial parameters governing soil behavior. The utilized equations for determining the FSP and ASWV, as well as the suggested method in this study, along with their corresponding nomenclature, are outlined in Table 1. Among these, the relationship between the ASWV and the FSP, denoted as V_{sa} and T, respectively, is expressed in Eq. (36), a well-known equation in the literature.

$$V_{sa} = \frac{4H}{T}. \tag{36}$$

The two equations to be used in the methods, nomenclatured M1 and M2 in Table 1, are widely used in the literature [Takabatake *et al.*, 2019]. According to the Mexican earthquake code, the equations provided in the method nomenclatured as M3 in Table 1 are used in the period calculation [Tena-Colunga *et al.*, 2009], where G_i and ρ_i are the shear modulus and mass density of the ith layer of thickness and

$$w_i = \frac{\sum_{j=1}^{i} d_j/G_j}{\sum_{j=1}^{n} d_j/G_j}; \quad i = 1, 2, \ldots, n \tag{37}$$

is a static approximation for the fundamental mode of soil vibration. According to the Japanese seismic design code, the FSP is determined using the equation provided

Table 1. Equations used in the calculation of the ASWV and FSP.

Method ID	Description	Equation
M1	The square root of the weighted average of shear velocities of layers	$V_{sa} = \sqrt{\frac{\sum_{i=1}^{n} d_i V_{si}^2}{H}}$
M2	The weighted average of shear velocities of layers	$V_{sa} = \frac{\sum_{i=1}^{n} d_i V_{si}}{H}$
M3	Mexican Earthquake Code	$T = 4\sqrt{\left(\sum_{i=1}^{n} \frac{d_i}{G_i}\right)\left(\sum_{i=1}^{n} \rho_i d_i (w_i^2 + w_i w_{i-1} + w_{i-1}^2)\right)}$
M4	Japan Earthquake Code	$T = \sqrt{32 \sum_{i=1}^{n} \frac{d_i \left(\frac{H_{i-1}+H_i}{2}\right)}{V_{si}^2}}$
M5	Turkish Earthquake Code	$V_{sa} = \frac{H}{\sum_{i}^{n} \frac{d_i}{V_{si}}}$
M6	Rayleigh method	$T = 2\pi \sqrt{\frac{\sum_{i=1}^{n} m_i \Delta_i^2}{\sum_{i=1}^{n} f_i \Delta_i}}$
M7- Proposed	*The relationship between peak point displacement and FSP*	$T = 5.515\left[\sum_{i=1}^{n} \sqrt{\frac{S_i}{\rho_i V_{si}^2}} d_i\right]$

in the method nomenclatured as M4 in Table 1 [Mariano *et al.*, 2005]. Here, H_i represents the depth of the ith layer. The equation provided in the method used to determine ASWV in NEHRP, BSSC, EC8 and T.S.C. is named as M5 in Table 1. One of the methods used to determine the FSP is the Rayleigh method, which has various applications in the literature [Dobry *et al.*, 1976]. Widely employed in seismic codes to find the fundamental periods of buildings, this method is adapted in this study to determine the FSP. The relation of the Rayleigh method for the determination of the FSP is designated as M6 in Table 1. Here, m, f, and Δ represent the mass, force, and displacement as defined in Eqs. (38)–(40), respectively,

$$m_i = \rho_i \frac{[d_i + d_{i+1}]}{2} \quad i = 1, 2, \ldots, n-1 \quad \text{and} \quad m_n = \frac{\rho_n d_n}{2}, \tag{38}$$

$$f_i = \frac{m_i(H - H_i)}{\sum m_i(H - H_i)} \quad i = 1, 2, \ldots, n, \tag{39}$$

$$\Delta_i = \Delta_{i-1} + \frac{Q_i}{\rho_i V_{si}^2} \quad i = 1, 2, \ldots, n \tag{40}$$

and furthermore, the shear force Q_i is presented in Eq. (41).

$$Q_i = \sum_{i=1}^{n} f_i. \tag{41}$$

The validity of the proposed equation is examined by applying it to calculate the ASWV and FSP for 10 different soil profiles. Details regarding the soil profiles utilized in the study are provided in this section.

3.1. *Example 1*

The first example examines a soil profile detailed in [Yoshida, 2015], featuring a total depth of 380 m and comprising 12 layers. The soil's characteristics are provided in Table 2. The table shows that shear wave velocities vary between 107 m/s and 1100 m/s.

Table 2. Soil profile properties for Example 1.

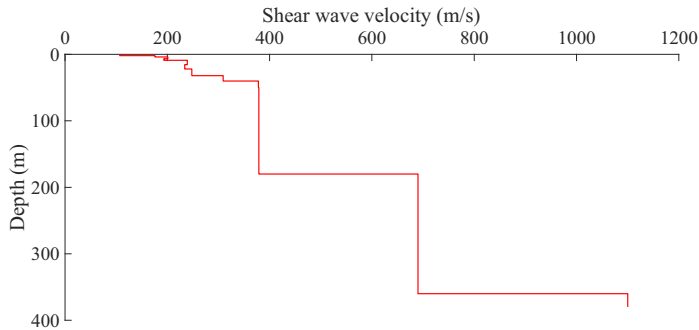| Layer no.	Layer's thickness (m)	SWV (m/s)
1	2	107
2	2	176
3	2.5	201
4	2.5	193
5	6.5	239
6	6.5	234
7	10	248
8	8	309
9	10	378
10	130	379
11	180	690
12	20	1100

Fig. 6.   Variation of SWV with depth for Example 1.

Figure 6 illustrates the relationship between depth and SWV graph for the soil profile presented in Table 2.

3.2. *Example 2*

The characteristics of a soil profile, comprising five layers and spanning a total depth of 35.5 m, have been sourced from the literature [Ozkan, 2017] and are detailed in Table 3. In this soil profile, the SWV ranges from 120 m/s to 500 m/s.

Figure 7 illustrates the variation in SWV with depth for the soil profile detailed in Table 3. As depicted in the figure, the SWV increases with depth.

Table 3.   Soil profile properties for Example 2.

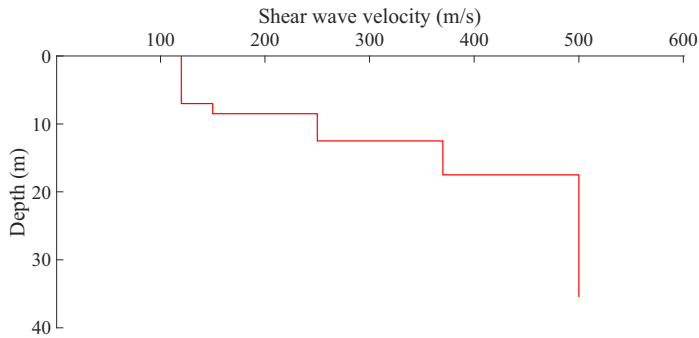| Layer no.	Layer's thickness (m)	SWV (m/s)
1	7	120
2	1.5	150
3	4	250
4	5	370
5	18	500

Fig. 7.   Variation of SWV with depth for Example 2.

3.3. *Example 3*

The characteristics of the soil profile, comprising five layers and obtained from Jia [2018], are outlined in Table 4. As indicated in the table, shear wave velocities exhibit a range between 360 m/s and 2400 m/s.

Figure 8 illustrates the depth–SWV graph of the soil profile provided in Table 4. As depicted in the figure, the SWV increases with depth.

3.4. *Example 4*

The soil characteristics detailed in Takabatake *et al.* [2019] are presented in Table 5. The soil profile comprises five layers with a total thickness of 29 m. The SWV is 146.6 m/s in the first layer and 472.9 m/s in the fifth layer.

Table 4. Soil profile properties for Example 3.

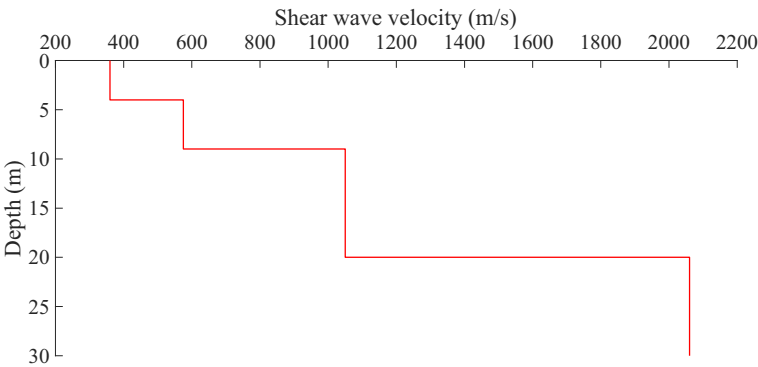| Layer no.	Layer's thickness (m)	SWV (m/s)
1	4	360
2	5	575
3	11	1050
4	10	2060

Fig. 8. Variation of SWV with depth for Example 3.

Table 5. Soil profile properties for Example 4.

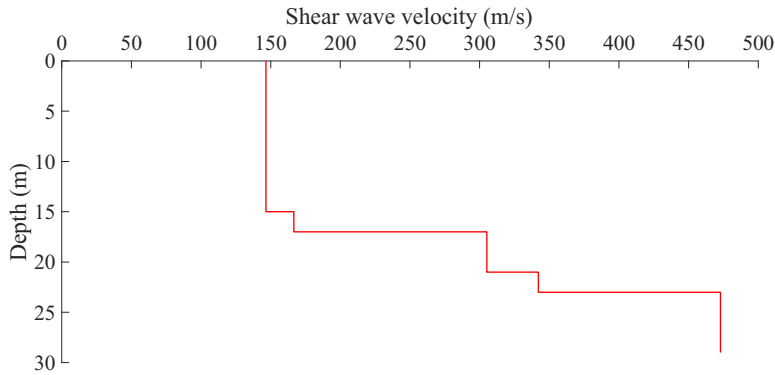| Layer no.	Layer's thickness (m)	SWV (m/s)
1	15	146.6
2	2	166.6
3	4	305.2
4	2	342.2
5	6	472.9

Fig. 9. Variation of SWV with depth for Example 4.

Figure 9 illustrates the variation of SWV with depth. As seen from the figure, there is a corresponding increase in SWV as depth increases.

3.5. *Example 5*

The soil profile properties provided in Table 6 are obtained from the literature [Vijayendra *et al.*, 2010] and comprise 14 layers with a total layer thickness of 100.01 m. The SWV is 175.26 m/s in the first layer and 1899.51 m/s in the 14th layer.

Figure 10 illustrates the variation of SWV with depth. As depicted in the figure, an observable increase in SWV corresponds to the depth increase.

3.6. *Example 6*

The attributes of a soil profile, comprising six layers and spanning a total depth of 85 m, have been sourced from the literature [Hasanoglu, 2021] and are detailed in

Table 6. Soil profile properties for Example 5.

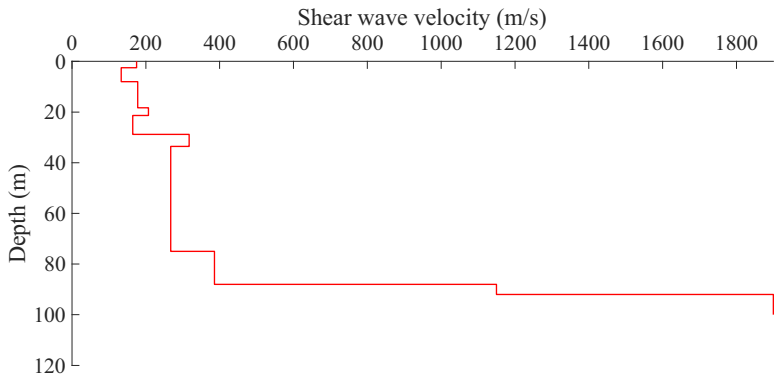| Layer no.	Layer's thickness (m)	SWV (m/s)
1	2.50	175.26
2	5.52	133.50
3	4.69	178.00
4	5.61	178.00
5	3.05	207.26
6	7.47	164.59
7	4.72	317.30
8	11.06	267.31
9	19.11	267.31
10	11.28	267.31
11	8.23	385.88
12	4.79	385.88
13	3.99	1149.71
14	7.99	1899.51

Fig. 10.   Variation of SWV with depth for Example 5.

Table 7.   Soil profile properties for Example 6.

Layer no.	Layer's thickness (m)	SWV (m/s)
1	3.5	140
2	8.5	140
3	9	200
4	16	200
5	23	375
6	25	500

Table 7. The table shows that shear wave velocities range between 140 m/s and 500 m/s.

Figure 11 illustrates the variation of SWV with depth. As depicted in the figure, an increase in SWV is evident in correlation with the depth increment.
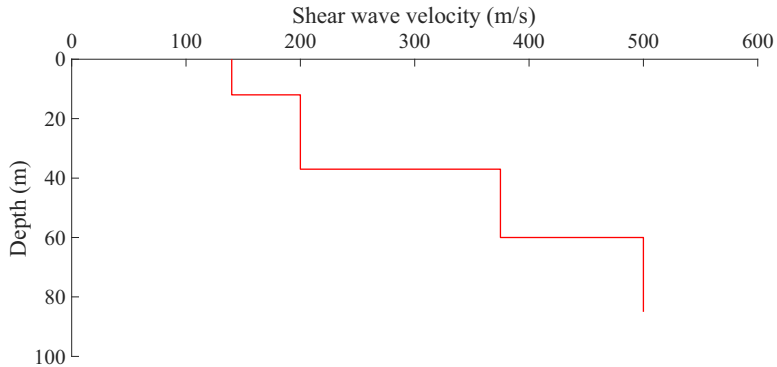

Fig. 11.   Variation of SWV with depth for Example 6.

Table 8. Soil profile properties for Example 7.

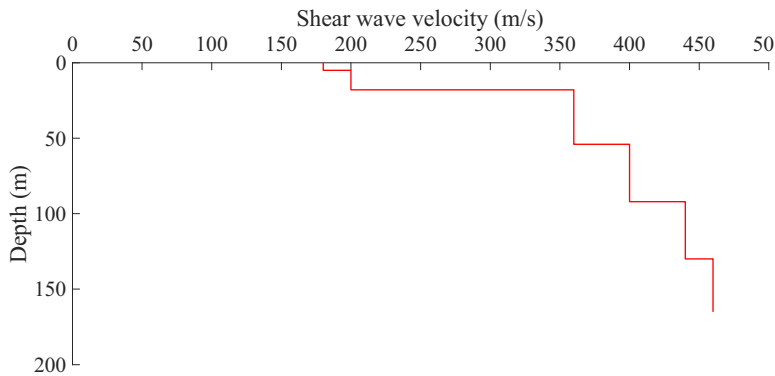| Layer no.	Layer's thickness (m)	SWV (m/s)
1	5	180
2	13	200
3	36	360
4	38	400
5	38	440
6	35	460

Fig. 12. Variation of SWV with depth for Example 7.

3.7. *Example 7*

Another example from the literature [Gullu and Hasanoglu, 2022] comprises six layers with a total layer thickness of 165 m. The soil profile characteristics are provided in Table 8, showing a SWV of 180 m/s in the first layer and 460 m/s in the sixth layer.

The variation of SWV with depth is depicted in Fig. 12. As shown, there is a noticeable increase in SWV with increasing depth.

Table 9. Soil profile properties for Example 8.

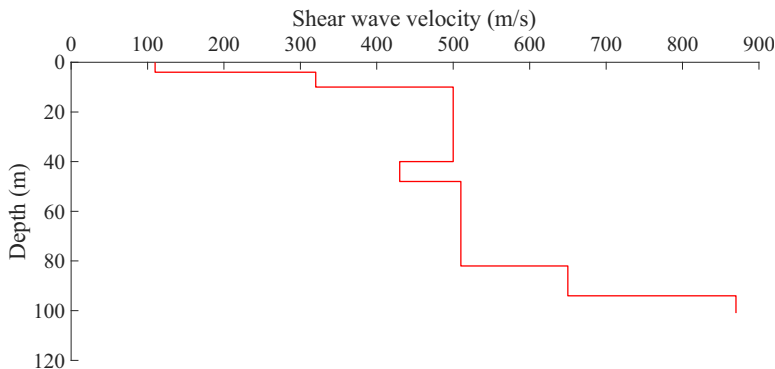| Layer no.	Layer's thickness (m)	SWV (m/s)
1	4	110
2	6	320
3	30	500
4	8	430
5	34	510
6	12	650
7	7	870

Fig. 13.   Variation of SWV with depth for Example 8.

3.8. *Example 8*

This example examines a soil profile featuring a total depth of 101 m and comprising seven layers, as sourced from the literature [Kokusho and Ishizawa, 2021]. Within this soil profile, as presented in Table 9, the SWV ranges from 110 m/s to 870 m/s.

Figure 13 illustrates the variation of SWV with depth. As shown, there is a noticeable increase in SWV as depth increases.

3.9. *Example 9*

In this example, a soil profile obtained from station 3126 in the Antakya district of Hatay, recorded by the AFAD organization that monitors strong ground movements in Turkey, is considered [AFAD, 2023]. The soil profile, as presented in Table 10, comprises 10 layers with a total depth of 34.82 m. For this soil profile, the SWV ranges from 275 m/s to 650 m/s, as illustrated in Fig. 14.

3.10. *Example 10*

In this example, a soil profile obtained from station 4621, located in the Dulkadiroglu district of Kahramanmaras, recorded by the AFAD organization that monitors

Table 10.   Soil profile properties for Example 9.

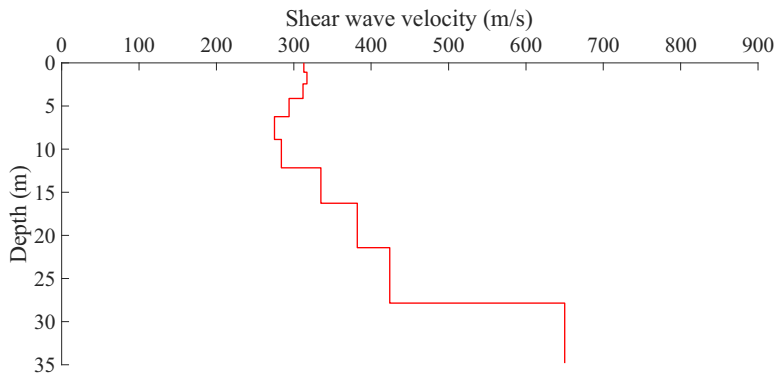| Layer no.	Layer's thickness (m)	SWV (m/s)
1	1.08	313
2	1.35	317
3	1.69	312
4	2.11	294
5	2.63	275
6	3.30	284
7	4.11	335
8	5.15	382
9	6.44	424
10	6.96	650

Fig. 14.   Variation of SWV with depth for Example 9.

Table 11.   Soil profile properties for Example 10.

Layer no.	Layer's thickness (m)	SWV (m/s)
1	2.39	698
2	2.99	717
3	3.74	683
4	4.68	601
5	5.84	620
6	7.30	835
7	9.13	1013

strong ground motions in Turkey, is considered. The soil profile comprises seven layers with a total depth of 36.07 m.

For this soil profile, given in Table 11, the SWV ranges from 601 m/s to 1013 m/s.

Figure 15 illustrates the variation of SWV with depth. As depicted in the figure, there is an observable increase in SWV in correlation with the depth increment.
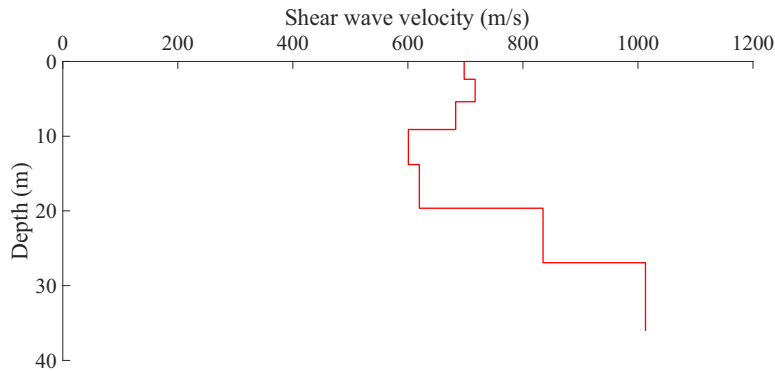

Fig. 15.   Variation of SWV with depth for Example 10.

4. Results and Discussion

In order to evaluate the validation of the results obtained from the Modified Finite Element Transfer Matrix Method, referred to as exact results, SAP2000 software using the FEM is used. The corresponding outcomes are shown in Table 12. Generally, the results obtained from SAP2000 are consistent with those from the Modified Finite Element Transfer Matrix Method, with slight differences in some examples thought to be due to the shape functions used by SAP2000. Additionally, the TFT program was utilized to validate the exact results, confirming that the obtained FSP results are exactly the same as the exact results. Detailed information on finding the fundamental site period using transfer functions can be found in the literature [Kramer, 1996]. The first peak of the transfer function gives the fundamental frequency. From the fundamental frequency, the fundamental site period is determined. Moreover, the example provided by Yoshida is solved by Yoshida with the continuous FEM and the result obtained from here coincides exactly with the Modified Finite element transfer matrix method.

The seven methods outlined in Table 1, including the proposed method, are applied to 10 different soil profiles, and the resulting data are presented in this section. The outcomes obtained through these various methods are summarized in Tables 13 and 14. Transfer functions and the Modified Finite Element Transfer Matrix Method [Ozturk and Bozdogan, 2017] are employed for the exact solution of

Table 12.   Verification of SAP2000 and exact results for fundamental site period.

	Yoshida	Ozkan	Junbo Jia	Takabate	Vijendra
SAP2000	2.578	0.377	0.0994	0.505	1.278
Exact	2.5110	0.3760	0.0993	0.508	1.260
	Hasanoglu	Gullu	Kokusho	Antakya	Dulkadiroglu
SAP2000	0.987	1.535	0.740	0.326	0.1773
Exact	0.9813	1.5319	0.7363	0.3254	0.1772

Table 13.   Fundamental soil periods calculated by different methods.

	M1	M2	M3	M4	M5	M6	M7	Exact
Yoshida	2.575	2.766	2.255	2.699	3.300	2.5890	2.5504	2.5110
Özkan	0.358	0.390	0.373	0.414	0.536	0.3720	0.3928	0.3760
Junbo Jia	0.087	0.098	0.090	0.108	0.141	0.0999	0.1031	0.0993
Takabate	0.410	0.462	0.516	0.514	0.583	0.5140	0.4917	0.5080
Vijendra	1.3257	1.3794	1.2074	1.3197	1.5090	1.2654	1.2425	1.2600
Hasanoglu	0.9650	1.0479	0.9259	1.0548	1.2982	0.9906	0.9837	0.9813
Gullu	1.6566	1.6889	1.3853	1.5763	1.8009	1.5392	1.4916	1.5319
Kokusho	0.7559	0.7842	0.5776	0.7563	0.9076	0.7436	0.7094	0.7363
Antakya	0.3258	0.3422	0.3240	0.3342	0.3725	0.3265	0.3226	0.3254
Dulkadiroglu	0.1813	0.1849	0.1785	0.1922	0.1801	0.1782	0.1723	0.1772

Table 14.   ASWV calculated by different methods.

	M1	M2	M3	M4	M5	M6	M7	Exact
Yoshida	590	550	674	563	461	596	587	605
Özkan	397	364	381	343	265	362	382	378
Junbo Jia	1379	1224	1333	1111	851	1164	1201	1208
Takabate	283	251	225	226	199	236	226	228
Vijendra	266	255	292	267	233	283	278	279
Hasanoglu	352	324	367	322	262	346	343	346
Gullu	398	391	476	419	366	442	429	431
Kokusho	534	515	699	534	445	569	543	549
Antakya	428	407	430	417	374	432	427	428
Dulkadiroglu	796	780	808	751	801	837	810	814

the FSPs. The results achieved using the transfer functions and the Modified Finite Element Transfer Matrix Method yielded exactly the same results across all discussed examples.

To assess the convergence of the period values presented in Table 13 to the actual period value, the period values are evaluated using the true fractional relative error (TFRE) given by [Chapra, 2011].

$$M(n)_{\text{nor}} = \frac{T_{M(n)}}{T_{\text{exact}}} - 1 \quad (n = 1, 2, \ldots, 7). \tag{42}$$

TFRE values for methods M1, M2, M3, M4, M5, M6, and M7 are depicted in Figs. 16–22, respectively.

Figure 16 shows that the M1 method yields lower period values for soil profiles Ozkan, Junbo Jia, Takabate, and Hasanoglu compared to the exact period values. Conversely, it produces higher period values for soil profiles Yoshida, Vijendra,
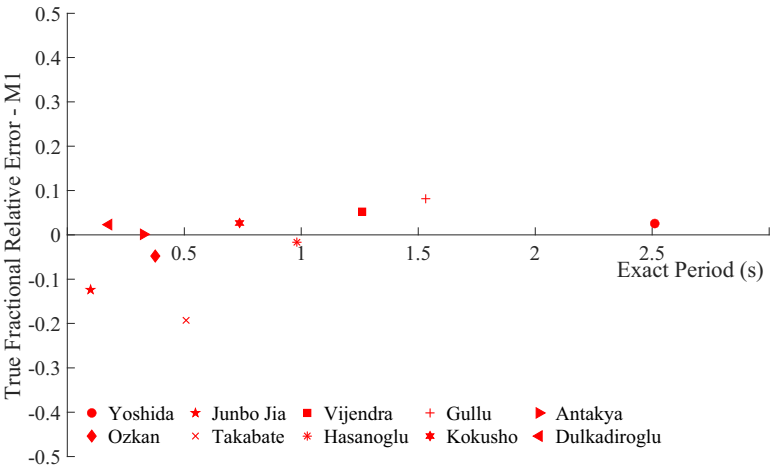

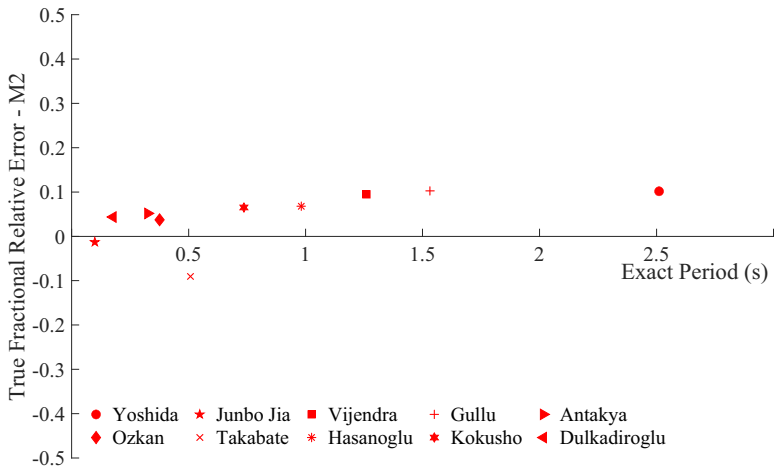Fig. 16.   TFRE values of the M1 method for 10 different soil profiles.

Fig. 17.   TFRE values of the M2 method for 10 different soil profiles.

Gullu, Kokusho, Antakya and Dulkadiroglu. The method exhibits its highest error when applied to the Takabate soil profile.

As observed in Fig. 17, the M2 method resulted in lower than the exact period values for the Junbo Jia and Takabate soil profiles, while it gives higher period values for all other soil profiles.

As evident from Fig. 18, the periods calculated by the M3 method closely align with the exact period values for the Ozkan, Takabate, Antakya and Dulkadiroglu soil profiles. Conversely, lower period values are calculated for the remaining soil profiles.
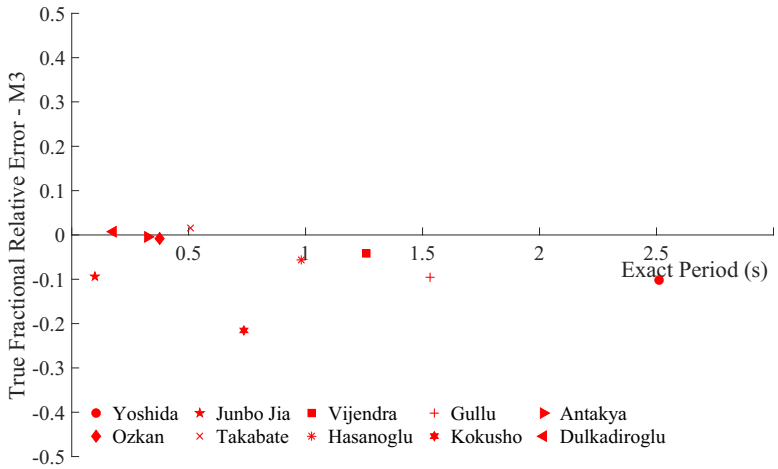

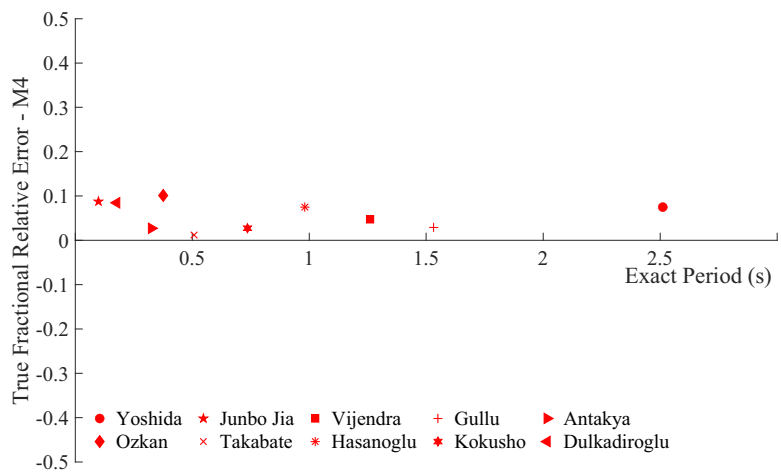Fig. 18.   TFRE values of the M3 method for 10 different soil profiles.

Fig. 19.   TFRE values of the M4 method for 10 different soil profiles.

The values obtained using the M4 method are presented in Fig. 19. While the M4 model provides the closest match for the Takabate soil profile, it yields period values above the exact period values for the remaining soil profiles.

Figure 20 presents a graph of the normalized period values for the M5 method. As can be seen from the graph, while the M5 model provides the closest match for the Dulkadiroglu soil profile, significant error rates are observed across all remaining soil profiles.

Figure 21 presents the calculated values obtained using the M6 method. As observed in the graph, it is evident that the period values calculated by the M6 method closely approximate the exact period values.
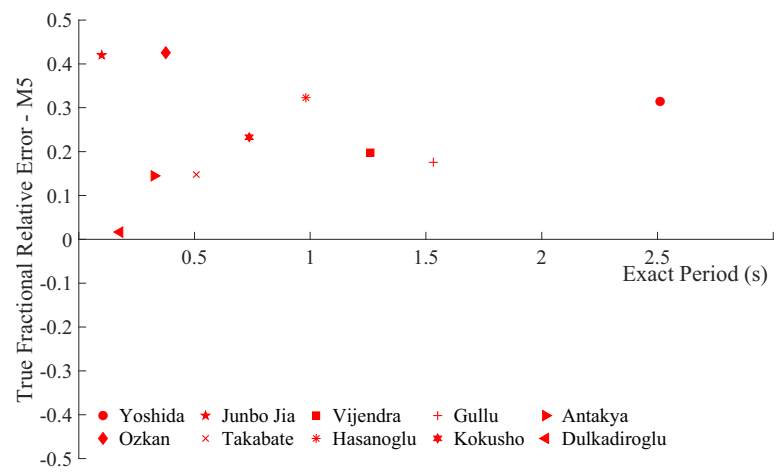

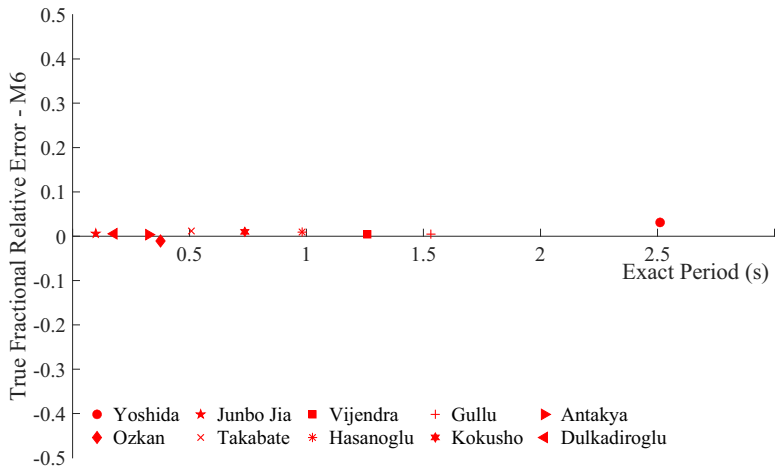Fig. 20.   TFRE values of the M5 method for 10 different soil profiles.

Fig. 21.   TFRE values of the M6 method for 10 different soil profiles.

Figure 22 presents the graph illustrating the normalized period values calculated using the M7 method. Upon examining the graph, it becomes evident that the period values calculated by the M7 method closely align with the exact period values.

Table 15 provides the error rates of the FSPs determined using seven different methods for 10 different soil profiles. Furthermore, a graph depicting these error rates in a more comprehensible manner, utilizing data from this table, is presented in Fig. 23.

To determine whether the period values obtained through different methods are lower or higher than the exact period values, the true percent relative error of the period values calculated by various methods to the actual period values are presented
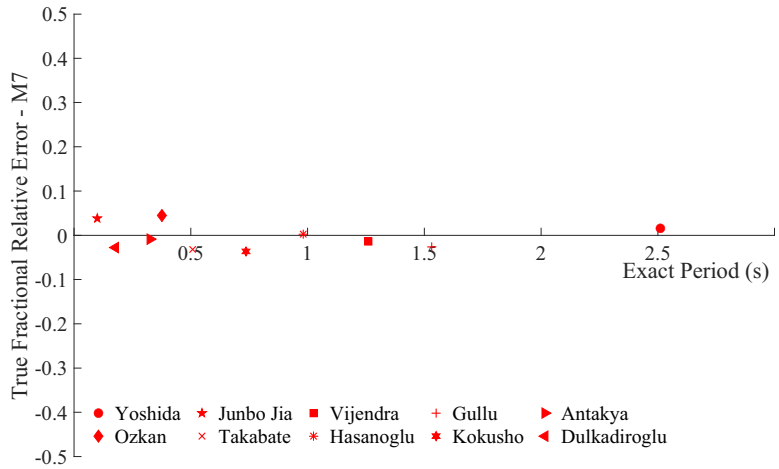

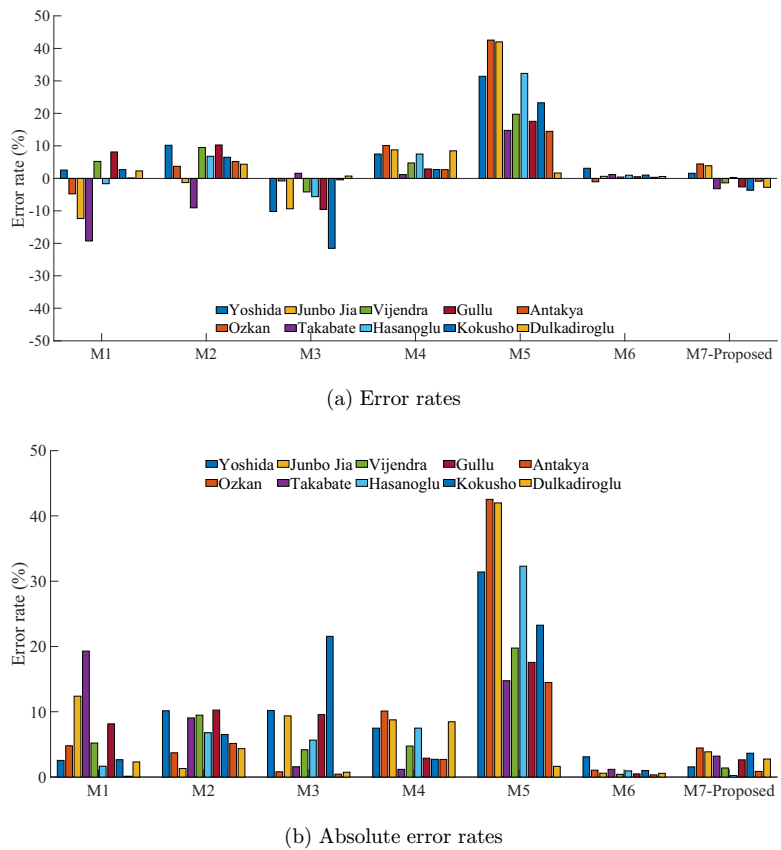Fig. 22.   TFRE values of the M7 method for 10 different soil profiles.

(a) Error rates

(b) Absolute error rates

Fig. 23.   Error and absolute error rates.

Table 15.   The true percent relative error of seven methods for 10 different soil profiles.

	Error rates (%)						
	M1	M2	M3	M4	M5	M6	M7
Yoshida	2.55	10.16	−10.20	7.49	31.42	3.11	1.57
Özkan	−4.79	3.72	−0.80	10.11	42.55	−1.06	4.47
Junbo Jia	−12.39	−1.31	−9.37	8.76	41.99	0.60	3.83
Takabate	−19.29	−9.06	1.57	1.18	14.76	1.18	−3.21
Vijendra	5.21	9.48	−4.17	4.74	19.76	0.43	−1.39
Hasanoglu	−1.66	6.79	−5.65	7.49	32.29	0.95	0.24
Gullu	8.14	10.25	−9.57	2.90	17.56	0.48	−2.63
Kokusho	2.66	6.51	−21.55	2.72	23.26	0.99	−3.65
Antakya 3126	0.12	5.16	−0.43	2.70	14.47	0.34	−0.86
Dulkadiroglu	2.31	4.35	0.73	8.47	1.64	0.56	−2.77

in Fig. 23(a), as illustrated by the graph that the estimated FSP values tend to be higher than the exact FSP values.

In Fig. 23(b), the absolute values of the error rates are utilized to compare the magnitude of errors. As depicted in this graph, the M5 method exhibited the least favorable outcomes compared to other methods. Notably, the M6 and M7 methods proposed in this study demonstrated the best level of performance.

5. Conclusion

This study proposes an equation to determine both the FSP and the ASWV. The proposed equation (M7) is derived by modeling the soil as an equivalent shear beam. The basic premise of the presented equation is based on the assumption that the FSP is proportional to the square root of the displacement at the top of the shear beam (at the soil surface). The relationship obtained between the FSP and the square root of the soil surface displacement in a single-layer soil profile has been generalized for multi-layer soil profiles by analyzing many soil profiles, employing the least squares method for this purpose. Consequently, an equation that allows the determination of the FSP is obtained by multiplying the square root of the peak displacement of the equivalent shear beam by a factor of 5.515. Within the scope of the study, FSPs and ASWV's for different soil profiles are solved with both the equation proposed in this study and the equations in the literature and seismic earthquake codes, and the results are compared with the exact solution. Three different methods are used for verification (exact solution): Transfer functions, FEM (SAP2000) and Modified Finite element transfer function method.

The study establishes that M2 and M3 yield more accurate outcomes than the conventional M1 used in seismic codes. Thus, it is inferred that M2 and M3 can be practically employed to more accurately determine the ASWV.

In addition to proposing a new equation (M7) to determine the FSP and AWSV, this paper proposes a special version of the Rayleigh method (M6), which is widely used in earthquake codes for the calculation of the fundamental period of buildings, adapted for the calculation of the FSP. The adapted version of the Rayleigh method proposed in this study is observed to yield results closest to the exact solution for calculating the FSP.

The results from the demonstrated examples emphasize the high accuracy of the proposed equation (M7). This method offers a reliable approach to computing the FSP and determining the ASWV. The error level of the method (M7) proposed in this study is within acceptable limits. Moreover, since M7 requires less computation and is more practical to use than M6, it is considered preferable.

ORCID

Kanat Burak Bozdogan https://orcid.org/0000-0001-7528-2418
Erdinc Keskin https://orcid.org/0000-0002-8728-2906

References

AFAD [2023] Turkish Accelerometric Database and Analysis System. Available at https://tadas.afad.gov.tr/[Accessed on 10 April 2023].

Aleshin, A. S. [2021] "On the disadvantages of the NEHRP soil classification," *Open J. Earthqu. Res.* **10**, 1–15, https://doi.org/ojer.2021.101001.

BSSC (Building Seismic Safety Council) [2003] 2003 Edition NEHRP Recommended Provisions for Seismic Regulations for New Buildings and Other Structures, Part 1: Provisions (FEMA 450).

Chapra, S. C. [2011] *Applied Numerical Methods with MATLAB for Engineering and Science*, 3rd edition (WCB/McGraw-Hill, New York).

Dobry, R., Oweis, I. and Urzua, A. [1976] "Simplified procedures for estimating the fundamental period of a soil profile," *Bull. Seismol. Soc. Amer.* **66**, 1293–1321.

Dong-Kwan, K. [2019] "Evaluation of average shear-wave velocity estimation methods of multi-layered strata considering site period," *J. Earthqu. Eng. Soc. Korea* **23**, 191–199, https://doi.org/10.5000/eesk.2019.23.3.191.

Eurocode8 [2004] Design of Structures for Earthquake Resistance, Part 1: General Rules, Seismic Actions and Rules For Buildings (EN 1998–1:2004, Brussels, Belgium).

Fadayi Asiabsary, K., Hadiani, N., Eghbali, A. H. and Sadreddini, S. M. A. [2023] "Effects of inclination of longitudinal and vertical acceleration components of near-field earthquake records on seismic responses of pile foundation-superstructure systems in liquefiable soil bed," *J. Earthqu. Tsunami*, https://doi.org/10.1142/S1793431123500422.

Genovese, F., Aliberti, D., Biondi, G. and Cascone, E. [2019a] "A procedure for the selection of input ground motion for 1D seismic response analysis," in *Earthquake Geotechnical Engineering for Protection and Development of Environment and Constructions* (CRC Press), pp. 2591–2598.

Genovese, F., Aliberti, D., Biondi, G. and Cascone, E. [2019b] "Geotechnical aspects affecting the selection of input motion for seismic site response analysis," *Proc. 7th Computational Methods in Structural Dynamics and Earthquake Engineering* (Crete, Greece), pp. 24–26, https://doi.org/10.7712/120119.6909.19616.

Genovese, F., Aliberti, D., Biondi, G. and Cascone, E. [2020] "Influence of soil heterogeneity on the selection of input motion for 1D seismic response analysis," in *Geotechnical Research for Land Protection and Development: Proceedings of CNRIG*, Vol. 7 (Springer International Publishing), pp. 694–704.

Genovese, F., Biondi, G., Cascone, E. and Muscolino, G. [2023a] "Energy-compatible modulating functions for the stochastic generation of fully non-stationary artificial accelerograms and their effects on seismic site response analysis," *Earthqu. Eng. Struct. Dynam.* **52**(9), 2682–2707, https://doi.org/10.1002/eqe.3889.

Genovese, F., Muscolino, G. and Palmeri, A. [2023b] "Effects of stochastic generation on the elastic and inelastic spectra of fully non-stationary accelerograms," *Probab. Eng. Mech.* **71**, 103377, https://doi.org/10.1016/j.probengmech.2022.103377.

Gullu, A. and Hasanoglu, S. [2022] "A statistical investigation to determine dominant frequency of layered soil profiles," *Turk. J. Eng.* **6**(2), 95–105.

Haque, M. F. and Ahmed Ansary, M. [2023]. "Seismically evaluate liquefaction-induced steel tunnel–sand–pile interaction (tspi) response," *J. Earthqu. Tsunami* **17**(5), 2350021, https://doi.org/10.1142/S1793431123500215.

Hasanoglu, S. [2021] "An approximate method to estimate fundamental site period by utilising V_{s30} and bedrock depth," Istanbul Technical University Graduate School, Turkey (in Turkish).

Hoseini, S. S., Ghanbari, A., Davoodi, M. and Kamal, M. [2019] "The effect of foundation soil behavior on seismic response of long bridges," *Geomech. Eng.* **17**(6), 583–595, https://doi.org/10.12989/GAE.2019.17.6.583.

Huynh, V. Q., Nguyen, T. K. and Nguyen, X. H. [2021] "Seismic analysis of soil-structure interaction: experimentation and modeling," *Geomech. Eng.* **27**(2), 115–121, https://doi.org/10.12989/GAE.2021.27.2.115

Jia, J. [2018] *Soil Dynamic and Foundation Modeling: Offshore and Earthquake Engineering* (Springer International Publishing, Switzerland), https://doi.org/10.1007/978-3-319-40358-8.

Jiang, S., Du, C. and Sun, L. [2018] "Numerical analysis of sheet pile wall structure considering soil-structure interaction," *Geomech. Eng.* **16**(3), 309–320, https://doi.org/10.12989/GAE.2018.16.3.309.

Jin, L., Du, L. and Wang, H. [2021]. "Dynamic interaction of two independent SDOF oscillators supported by a flexible foundation embedded in a half-space: Closed-form analytical solution for incident plane SH-waves," *J. Earthqu. Tsunami* **15**(06), 2150026, https://doi.org/10.1142/S1793431121500263.

Kokusho, T. and Ishizawa, T. [2021] "Site amplification during strong earthquakes investigated by vertical array records," *Geosciences* **11**, 510, https://doi.org/10.3390/geosciences11120510.

Kramer, S. L. [1996] *Geotechnical Earthquake Engineering*, Prentice–Hall International Series in Civil Engineering and Engineering Mechanics (Prentice-Hall, New Jersey).

Lee, V. W. and Trifunac, M. D. [2010] "Should average shear-wave velocity in the top 30 m of soil be used to describe seismic amplification," *Soil Dynam. Earthqu. Eng.* **30**, 1250–1258, https://doi.org/j.soildyn.2010.05.007.

Luzi, L., Puglia, R., Pacor, E., Gallipoli, M., R., Bindi, D. and Mucciarelli [2011] "Proposal for a soil classification based on parameters alternative or complementary to $V_{s,30}$," *Bull. Earthqu. Eng.* **9**, 1877–1898, https://doi.org/10.1007/s10518-011-9274-2.

Mariano, E. M., Nakashima, M. and Mosalam, K. M. [2005] "Comparison of European and Japanese seismic design of steel building structures," *Eng. Struct.* **27**, 827–840.

Miao, Y. and Wang, S. Y. [2018] "A study on the natural periods of soil site based on ground motion data from KiK-net in Japan," *Proc. GeoShanghai 2018 Int. Conf.: Advances in Soil Dynamics and Foundation Engineering*, Singapore, https://doi.org/10.1007/978-981-13-0131-5_4.

Ngo, V. L., Kim, J. M. and Lee, C. [2019] "Influence of structure-soil-structure interaction on foundation behavior for two adjacent structures," *Geo-Centrifuge Experi. Geomech. Eng.* **19**, 407–420, https://doi.org/10.12989/gae.2019.19.5.407.

Ozkan, M. Y. [2017] *Introduction of Soil Dynamics* (Nobel Publishing, Istanbul) (in Turkish).

Ozturk, D. and Bozdogan, K. B. [2017] "A method for determination of the fundamental period of layered soil profiles," *J. Appl. Comp. Mech.* **3**(4), 267–273.

Ozturk, K. F., Cakir, T. and Araz, O. [2023] "Influences of wall configurations on earthquake behavior of cantilever retaining walls considering soil-structure interaction effects," *J. Earthqu. Tsunami* **17**(01), 2250021, https://doi.org/10.1142/S179343112250021X.

Parla, R. and Somala, S. N. [2022] "Seismic ground motion amplification in a 3D sedimentary Basin: Source mechanism and intensity measures," *J. Earthqu. Tsunami* **16**(04), 2250008, https://doi.org/10.1142/S1793431122500087.

Pitilakis, K., Riga, E. and Anastasiadis, A. [2013] "New code site classification, amplification factors and normalised response spectra based on a worldwide ground-motion database," *Bull. Earthqu. Eng.* **11**, 925–966, https://doi.org/s10518-013-9429-4.

Raheem, S. E. A., Alazrak, T. M. A., Abdelshafy, A. G. A., Ahmed, M. M. and Gamal, Y. A. S. [2021] "Seismic pounding between adjacent buildings considering soil-structure interaction," *Earthqu. Struct.* **20**(1), 55–70, https://doi.org/10.12989/EAS.2021.20.1.055.

Sawada, S. [2004] "A Simplified equation to approximate natural period of layered ground on the elastic bedrock for seismic design of structures," *13th World Conf. Earthquake Engineering*, Vancouver, B.C., Canada.

Sbartai, B. [2020] "A polynomial mathematical tool for foundation-soil-foundation interaction," *Geomech. Eng.* **23**(6), 547–560, https://doi.org/10.12989/GAE.2020.23.6.547.

Shi, Y., He, H. J. and Miao, Y. [2022] "Multidirectional linear site response analysis by applying the SBSR technique to KiK-net data," *J. Earthqu. Tsunami* **16**(02), 2140005, https://doi.org/10.1142/S1793431121400054.

Takabatake, H., Kitada, Y., Takewaki, I. and Kishida, A. [2019] *Simplified Dynamic Analysis of High-Rise Buildings* (Springer Nature Singapore Pte Ltd), https://doi.org/10.1007/978-981-13-7185-1_1.

Tena-Colunga, A., Mena-Hernandez, U., Perez-Rocha, L. E, Javier, A., Ordaz, M. and Vilar, J. I. [2009] "Updated seismic design guidelines for model building code of Mexico," *Earthqu. Spectra* **25**(4), 869–898, https://doi.org/10.1193/1.3240413.

TSC (Turkish Seismic Code) [2018] Disaster and Emergency Management Presidency, Ankara, Turkey (In Turkish).

Van Cao, V. [2018] "Effect of soil-structure interaction on seismic damage of mid-rise reinforced concrete structures retrofitted by F.R.P. composites," *Earthqu. Struct.* **15**(3), 307–317, https://doi.org/10.12989/EAS.2018.15.3.307.

Vijayendra, K. V., Prasad, S. K. and Nayak, S. [2010] "Computation of fundamental period of soil deposit: A comparative study," *Indian Geotechnical Conference*, 2nd edition, December 16–18, Oxford, U.K.

Wang, S., Shi, Y., Jiang, W., Yao, E. and Miao, Y. [2018] "Estimating site fundamental period from shear-wave velocity profile," *Bull. Seismol. Soc. Amer.* **108**(6), 3431–3445, https://doi.org/10.1785/0120180103.

Yoshida, N. [2015] *Seismic Ground Response Analysis* (Springer, Dordrecht, Heidelberg, New York, London), https://doi.org/10.1007/978-94-017-9460-2.

Yu, Y., Liu, Q. and Ding, H. [2023] "Sensitivity study of seismic amplification effect of large-scale Sichuan basin on key parameters during the great Wenchuan earthquake," *J. Earthqu. Tsunami* **17**(06), 2350023, https://doi.org/10.1142/S1793431123500239.

Yuebing, L., Yuze, H., Yang, L., Qushenglin, S. and Shuang, X. [2024] "Effect of site soil and bus bars on the seismic performance of an isolated power transformer," *J. Earthqu. Tsunami*, 2350039, https://doi.org/10.1142/S1793431123500392.

Zhang, H. and Zhao, Y. G. [2019] "A simple approach for estimating the fundamental mode shape of layered soil profiles," *J. Earthqu. Tsunami* **13**(01), 1950003, https://doi.org/10.1142/S1793431119500039.

Zhang, H. and Zhao, Y. G. [2021] "Investigation of relationship between the response and Fourier spectral ratios based on statistical analyses of strong-motion records," *J. Earthqu. Tsunami*, **15**(02), 2150008, https://doi.org/10.1142/S1793431121500081.

Zhang, H. and Zhao, Y. G. [2022] "Effect of radiation damping on the fundamental period of linear soil profiles," *J. Earthqu. Eng.*, https://doi.org///13632469.2021.1911884.

Zhao, B., Ho, J., Banerjee, S., Goh, S. H. and Lee, F. H. [2022]. "Modeling seismic-soil-pile interaction (SSPI) problems for large pile groups," *J. Earthqu. Tsunami* **16**(03), 2240005, https://doi.org/10.1142/S179343112240005X.